Perfectly Matched Layers for Elastodynamics: A New Absorbing Boundary Condition

W. C. Chew
Electromagnetics Laboratory
Department of Electrical and Computer Engineering
University of Illinois
Urbana, IL 61801

Q. H. Liu
Schlumberger-Doll Research
Old Quarry Road
Ridgefield, CT 06877

Abstract

The use of perfectly matched layers (PML) has recently been introduced by Berenger as a material absorbing boundary condition (ABC) for electromagnetic waves. In this paper, we will first prove that a fictitious elastodynamic material half-space exists that will absorb an incident wave for all angles and all frequencies. Moreover, the wave is attenuative in the second half-space. As a consequence, layers of such material could be designed at the edge of a computer simulation region to absorb outgoing waves. Since this is a material ABC, only one set of computer codes is needed to simulate an open region. Hence, it is easy to parallelize such codes on multiprocessor computers. For instance, it is easy to program massively parallel computers on the SIMD (single instruction multiple data) mode for such codes. We will show two and three dimensional computer simulations of the PML for the linearized equations of elastodyanmics. Comparison with Liao's ABC will be given.

1. Introduction

Simulation of elastic waves in inhomogeneous media is important in many applications such as seismic survey, acoustic well logging, and other nondestructive evaluation applications.

The finite-difference method is widely used to solve the elastodynamic equations. Earlier work uses the finite-difference method to solve the second order equations [1-3]. The staggered grid finite-difference algorithm for first-order elastodynamic equations was apparently used first by Madariaga [4]. This algorithm is essentially the same as the Yee's algorithm for Maxwell's equations [5], and is now the most popular finite-difference scheme used for solving elastodynamic problems [6–12]. With the advent of massively parallel computers, the finite-difference method has recently been applied to model large scale three-dimensional wave propagation problems in borehole environments [13–16].

To use the finite-difference method to solve wave propagation problems in unbounded domain, artificial boundary conditions have to be used to eliminate the reflections from the edges of the finite computation domain. Lindman's, Liao's, and Higdon's boundary conditions have been used successfully in 2-D and 3-D simulations [8-18].

The use of perfectly matched layers (PML) as an absorbing boundary condition has been recently introduced for electromagnetic waves by Berenger [19]. Recently, Chew and Weedon [20] have interpreted the perfectly matched layers as coordinate stretching in frequency domain. Since the stretching variables are complex, they necessitate the splitting of Maxwell's equations in the time domain. The PML is shown to be of extremely wide bandwidth, and is capable of absorbing static electromagnetic fields as well [21].

A perfectly matched interface is an interface between two half spaces, one of which is lossy, but the interface does not reflect a plane wave for all frequencies and all angles of incidence. The loss of the wave in the lossy half space is in the direction normal to the interface.

In this paper, we will first demonstrate that a perfectly matched interface can also be designed for the equations of elastodynamics. This perfectly matched interface can be used to make PML, and used as material absorbing boundary conditions at the edge of a numerical simulation scheme to emulate an infinite region.

Material absorbing boundary conditions are useful for parallel computation since only one set of equations, and hence only one set of codes, need be written for numerical simulation. This is

File:pmie.tex, Date:April 3, 1996, accepted for publication by *J. Comp. Acoust.*

particularly suited for programming massively parallel computers in the SIMD (single instruction multiple data) mode [20]. Moreover, this boundary condition is stable when the Courant condition (also known as the Courant, Friedrichs, and Levy (CFL) condition) is satisfied [22]. Unlike the Liao's ABC [17], the computation need not be performed in double precision.

We will use coordinate stretching to introduce the perfectly matched layers. The manner with which coordinate stretching engenders losses in a medium can be easily understood as follows: Given a plane wave propagating in a lossless medium described by e^{ikx}, a coordinate stretching is a change of variable by letting $x = x'(a+i\alpha)$. Then e^{ikx} becomes $e^{ikax'-k\alpha x'}$. In other words, a wave becomes attenuative in the stretched x' coordinate if the stretching variable is complex.

2. Elastodynamics for Stretched Coordinates

To describe the equations of elastodynamics in a stretched coordinate system, we describe a nabla operator for stretched coordinates as

$$\nabla_e = \hat{x}\frac{1}{e_x}\partial_x + \hat{y}\frac{1}{e_y}\partial_y + \hat{z}\frac{1}{e_z}\partial_z. \tag{1}$$

The equations of motion for linearized elastodynamics are

$$-\rho\partial_t^2\mathbf{u} = \nabla_e \cdot \overline{\boldsymbol{\tau}}, \tag{2}$$

$$\overline{\boldsymbol{\tau}} = \lambda\overline{\mathbf{I}}(\nabla_e \cdot \mathbf{u}) + \mu(\nabla_e\mathbf{u} + \mathbf{u}\nabla_e), \tag{3}$$

where $\mathbf{u}\nabla_e$ is the transpose of $\nabla_e\mathbf{u}$, and $\overline{\mathbf{I}}$ is the identity matrix. In the frequency domain, the above could be written as

$$-\omega^2\rho\mathbf{u} = \nabla_e \cdot \overline{\boldsymbol{\tau}}, \tag{4}$$

$$\overline{\boldsymbol{\tau}} = \lambda\overline{\mathbf{I}}(\nabla_e \cdot \mathbf{u}) + \mu(\nabla_e\mathbf{u} + \mathbf{u}\nabla_e). \tag{5}$$

Assuming a plane wave solution that

$$\mathbf{u} = \mathbf{u}_0 e^{i\mathbf{k}\cdot\mathbf{r}}, \tag{6a}$$

$$\overline{\boldsymbol{\tau}} = \overline{\boldsymbol{\tau}}_0 e^{i\mathbf{k}\cdot\mathbf{r}}, \tag{6b}$$

we have for a homogeneous medium that

$$-\omega^2\rho\mathbf{u} = i\mathbf{k}_e \cdot \overline{\boldsymbol{\tau}}, \tag{7}$$

$$\overline{\boldsymbol{\tau}} = i\lambda\overline{\mathbf{I}}(\mathbf{k}_e \cdot \mathbf{u}) + i\mu(\mathbf{k}_e\mathbf{u} + \mathbf{u}\mathbf{k}_e). \tag{8}$$

For a stretched coordinate system,

$$\mathbf{k}_e = \hat{x}\frac{k_x}{e_x} + \hat{y}\frac{k_y}{e_y} + \hat{z}\frac{k_z}{e_y}. \tag{9}$$

Combining (7) and (8), we have

$$\omega^2\rho\mathbf{u} = \lambda\mathbf{k}_e\mathbf{k}_e \cdot \mathbf{u} + \mu\mathbf{k}_e \cdot \mathbf{k}_e\mathbf{u} + \mu\mathbf{k}_e\mathbf{k}_e \cdot \mathbf{u}. \tag{10}$$

If we assume the wave to be purely transverse, we have $\mathbf{k}_e \cdot \mathbf{u} = 0$, and then the dispersion relation for transverse or shear waves is

$$k_s^2 = \omega^2\rho/\mu = \mathbf{k}_e \cdot \mathbf{k}_e. \tag{11}$$

Written explicitly, it is

$$k_s^2 = \frac{1}{e_x^2}k_x^2 + \frac{1}{e_y^2}k_y^2 + \frac{1}{e_z^2}k_z^2. \tag{12}$$

The dispersion relation could be satisfied by

$$k_x = k_s e_x \sin\theta \cos\phi, \tag{13a}$$

$$k_y = k_s e_y \sin\theta \sin\phi, \tag{13b}$$

$$k_z = k_s e_z \cos\theta. \tag{13c}$$

Notice that in the above, e_x, e_y, and e_z can be complex numbers in the frequency domain. Hence, k_x, k_y, and k_z can be complex corresponding to decaying waves even when k_s is real.

Equation (10) can be written alternatively as

$$\omega^2 \rho \mathbf{u} = (\lambda + 2\mu)\mathbf{k}_e \mathbf{k}_e \cdot \mathbf{u} - \mu \mathbf{k}_e \times \mathbf{k}_e \times \mathbf{u}. \tag{14}$$

If the wave is longitudinal such that $\mathbf{k}_e \times \mathbf{u} = 0$, and $\mathbf{u} = \alpha \mathbf{k}_e$, then, the dispersion relation for longitudinal or compressional wave is

$$k_p^2 = \omega^2 \rho / (\lambda + 2\mu) = \mathbf{k}_e \cdot \mathbf{k}_e, \tag{15}$$

which is satisfied by

$$k_x = k_p e_x \sin\theta \cos\phi, \tag{16a}$$

$$k_y = k_p e_y \sin\theta \sin\phi, \tag{16b}$$

$$k_z = k_p e_z \cos\theta. \tag{16c}$$

The same statement for Equation (13) applies here.

3. A Single Interface Problem

Assume a plane wave incident on a plane interface between two solid half spaces. Without loss of generality, we can assume that the xz plane coincides with the plane of incidence so that $\partial/\partial y = 0$.

When the incident wave is an SH wave, it is completely equivalent to the electromagnetic case. Hence, we will only consider the case when the incident wave is an SV or P wave.

For a homogeneous medium, the equation of elastodynamics can be written as

$$\omega^2 \rho \mathbf{u} = (\lambda + 2\mu)\nabla_e \nabla_e \cdot \mathbf{u} - \mu \nabla_e \times \nabla_e \times \mathbf{u}. \tag{17}$$

We can let

$$\mathbf{u} = \nabla_e \phi + \nabla_e \times \boldsymbol{\psi}. \tag{18}$$

ϕ will be used to describe compressional waves while $\boldsymbol{\psi}$ is used to describe shear waves. Without loss of generality, we can let $\boldsymbol{\psi} = \hat{y}\psi$ describe SV waves in the xz plane. The boundary conditions at an interface require the continuity of u_x, u_z, τ_{zx} and τ_{zz}. In this case, we can easily show that

$$u_x = \underline{\partial}_x \phi - \underline{\partial}_z \psi, \quad u_z = \underline{\partial}_z \phi + \underline{\partial}_x \psi, \tag{19}$$

$$\tau_{zx} = 2\mu \underline{\partial}_x \underline{\partial}_z \phi + \mu(\underline{\partial}_x^2 \psi - \underline{\partial}_z^2 \psi), \tag{20}$$

$$\tau_{zz} = \lambda \nabla^2 \phi + 2\mu(\underline{\partial}_z^2 \phi + \underline{\partial}_x \underline{\partial}_z \psi, \tag{21}$$

where $\underline{\partial}_i = \frac{1}{e_i}\partial_i$ in the above for stretched coordinates. The continuity of the above quantities also follows directly from the equations of motion (2) and (3) in stretched coordinates.

3.1. P Wave Case

In this case, we can let the field in region 1 be

$$\phi_1 = A_1 e^{i\mathbf{k}_{1p}^- \cdot \mathbf{r}} + A_1 R_{pp} e^{i\mathbf{k}_{1p}^+ \cdot \mathbf{r}}, \tag{22}$$

$$\psi_1 = A_1 R_{vp} e^{i\mathbf{k}_{1v}^+ \cdot \mathbf{r}}. \tag{23}$$

In the above, $\mathbf{k}_{1p}^{\pm} = \hat{x}k_{1px} \pm \hat{z}k_{1pz}$, $\mathbf{k}_{1v}^{\pm} = \hat{x}k_{1vx} \pm \hat{z}k_{1vz}$, and $k_{1px}^2 + k_{1pz}^2 = k_{1p}^2$, $k_{1vx}^2 + k_{1vz}^2 = k_{1s}^2$. We have assumed that a P wave incident on the interface will generate both P and SV reflected waves. In region 2, we assume transmitted P and SV waves as well. Therefore, we have

$$\phi_2 = A_1 T_{pp} e^{i\mathbf{k}_{2p}^{-}\cdot\mathbf{r}}, \tag{24}$$

$$\psi_2 = A_2 T_{vp} e^{i\mathbf{k}_{2v}^{-}\cdot\mathbf{r}}. \tag{25}$$

For a non-slip interface, we require that u_x, u_z, τ_{zx} and τ_{zz} be continuous. For u_x continuous, we have

$$\frac{k_{1px}}{e_{1x}}(1 + R_{pp}) - \frac{k_{1vz}}{e_{1z}} R_{vp} = \frac{k_{2px}}{e_{2x}} T_{pp} + \frac{k_{2vz}}{e_{2z}} T_{vp}. \tag{26}$$

For u_z continuous, we have

$$\frac{k_{1pz}}{e_{1z}}(-1 + R_{pp}) + \frac{k_{1vx}}{e_{1x}} R_{vp} = -\frac{k_{2pz}}{e_{2z}} T_{pp} + \frac{k_{2vx}}{e_{2x}} T_{vp}. \tag{27}$$

For τ_{zx} continuous, we have

$$\begin{aligned} &-\frac{2\mu_1 k_{1px}k_{1pz}}{e_{1x}e_{1z}}(-1 + R_{pp}) - \mu_1 \left(\frac{k_{1vx}^2}{e_{1x}^2} - \frac{k_{1vz}^2}{e_{1z}^2}\right) R_{vp} \\ &\qquad = \frac{2\mu_2 k_{2px}k_{2pz}}{e_{2x}e_{2z}} T_{pp} - \mu_2 \left(\frac{k_{2vx}^2}{e_{2x}^2} - \frac{k_{2vz}^2}{e_{2z}^2}\right) T_{vp}. \end{aligned} \tag{28}$$

For τ_{zz} continuous, we have

$$\begin{aligned} &-\lambda_1 k_{1p}^2 (1 + R_{pp}) - 2\mu_1 \frac{k_{1pz}^2}{e_{1z}}(1 + R_{pp}) - 2\mu_1 \frac{k_{1vx}k_{1vz}}{e_{1x}e_{1z}} R_{vp} \\ &\qquad = -\lambda_2 k_{2p}^2 T_{pp} - 2\mu_2 \frac{k_{2pz}^2}{e_{2z}} T_{pp} + 2\mu_2 \frac{k_{2vx}k_{2vz}}{e_{2x}e_{2z}} T_{vp}. \end{aligned} \tag{29}$$

The above equations can be solved for the four unknowns R_{vp}, R_{pp}, T_{up} and T_{pp}. However, instead of going through the tedium of solving the above equations, we argue that if a perfectly matched interface exists, then $R_{vp} = R_{pp} = T_{vp} = 0$, and $T_{pp} = 1$. We can set R_{vp}, R_{pp}, T_{up} and T_{pp} to the aforementioned values, and see if contradiction arises. By so doing, we have from (26) to (29)

$$\frac{k_{1px}}{e_{1x}} = \frac{k_{2px}}{e_{2x}}, \tag{30}$$

$$\frac{k_{1pz}}{e_{1z}} = \frac{k_{2pz}}{e_{2z}}, \tag{31}$$

$$\frac{\mu_1 k_{1px}k_{1pz}}{e_{1x}e_{1z}} = \frac{\mu_2 k_{2px}k_{2pz}}{e_{2x}e_{2z}} \tag{32}$$

$$\lambda_1 k_{1p}^2 + 2\mu_1 \frac{k_{1pz}^2}{e_{1z}^2} = \lambda_2 k_{2p}^2 + 2\mu_2 \frac{k_{2pz}^2}{e_{2z}^2}. \tag{33}$$

The above equations are not consistent and we are to find the conditions under which they will be consistent.

By phase matching, we need $k_{1px} = k_{2px}$. Therefore, (30) could be satisfied by letting $e_{1x} = e_{2x}$. Furthermore, if we pick $\mu_1 = \mu_2, \lambda_1 = \lambda_2, \rho_1 = \rho_2$ then (31) to (33) could be satisfied even if $e_{1z} \neq e_{2z}$. Therefore, a perfectly matched interface exists for P wave if we let

$$\mu_1 = \mu_2, \quad \lambda_1 = \lambda_2, \quad \rho_1 = \rho_2, \quad e_{1x} = e_{2x}, \quad e_{1y} = e_{2y}, \quad e_{1z} \neq e_{2z}. \tag{34}$$

Therefore, the stretching variable in the direction normal to the interface need not be the same. For example, we can set $e_{1x} = e_{2x} = e_{1y} = e_{2y} = e_{1z} = 1$ and e_{2z} be a complex number. Then the upper half space is a normal medium, while in the lower half space, the wave will suffer an attenuation in the z direction.

3.2. SV Wave Case

In this case, we let the field in region 1 be

$$\psi_1 = A_1 e^{i\mathbf{k}_{1v}^{-}\cdot\mathbf{r}} + A_1 R_{vv} e^{i\mathbf{k}_{1v}^{+}\cdot\mathbf{r}}, \tag{35}$$

$$\phi_1 = A_1 R_{pv} e^{i\mathbf{k}_{1p}^{+}\cdot\mathbf{r}}. \tag{36}$$

We have assume that an SV wave incident on the interface will generate both P and SV reflected waves. In region 2, we assume transmitted P and SV waves as well as in (24) and (25). The correspondence to (26) to (29) becomes

$$\frac{k_{1px}}{e_{1x}} R_{pv} + \frac{k_{1vz}}{e_{1z}}(1 - R_{vv}) = \frac{k_{2px}}{e_{2x}} T_{pv} + \frac{k_{2vz}}{e_{2z}} T_{vv}, \tag{37}$$

$$\frac{k_{1pz}}{e_{1z}} R_{pv} + \frac{k_{1vx}}{e_{1x}}(1 + R_{vv}) = -\frac{k_{2pz}}{e_{2z}} T_{pv} + \frac{k_{2vx}}{e_{2x}} T_{vv}, \tag{38}$$

$$\begin{aligned} -\frac{2\mu_1 k_{1px} k_{1pz}}{e_{1x} e_{1z}} R_{pv} - \mu_1 \left(\frac{k_{1vx}^2}{e_{1x}^2} - \frac{k_{1vz}^2}{e_{1z}^2} \right) (1 + R_{vv}) \\ = \frac{2\mu_2 k_{2px} k_{2pz}}{e_{2x} e_{2z}} T_{pv} - \mu_2 \left(\frac{k_{2vx}^2}{e_{2x}^2} - \frac{k_{2vz}^2}{e_{2z}^2} \right) T_{vv}, \end{aligned} \tag{39}$$

$$\begin{aligned} -\lambda_1 k_{1p}^2 R_{pv} - 2\mu_1 \frac{k_{1pz}^2}{e_{1z}^2} R_{pv} - 2\mu_1 \frac{k_{1vx} k_{1vz}}{e_{1x} e_{1z}} (-1 + R_{vv}) \\ = -\lambda_2 k_{2p}^2 T_{pv} - 2\mu_2 \frac{k_{2pz}^2}{e_{2z}^2} T_{pv} + 2\mu_2 \frac{k_{2vx} k_{2vz}}{e_{2x} e_{2z}} T_{vv}. \end{aligned} \tag{40}$$

For a perfectly matched interface, we let $R_{pv} = R_{vv} = T_{pv} = 0$ and $T_{vv} = 1$. By so doing, we have

$$\frac{k_{1vz}}{e_{1z}} = \frac{k_{2vz}}{e_{2z}}, \tag{41}$$

$$\frac{k_{1vx}}{e_{1x}} = \frac{k_{2vx}}{e_{2x}}, \tag{42}$$

$$\mu_1 \left(\frac{k_{1vx}^2}{e_{1x}^2} - \frac{k_{1vz}^2}{e_{1z}^2} \right) = \mu_2 \left(\frac{k_{2vx}^2}{e_{2x}^2} - \frac{k_{2vz}^2}{e_{2z}^2} \right), \tag{43}$$

$$\mu_1 \frac{k_{1vx} k_{1vz}}{e_{1x} e_{1z}} = \mu_2 \frac{k_{2vx} k_{2vz}}{e_{2x} e_{2z}}. \tag{44}$$

The above could be satisfied by invoking the phase matching condition and requiring the same condition as (34). Therefore, a perfectly matched interface co-exists simultaneously for both P and SV waves incident.

4. Splitting of Elastodynamic Equations

In anticipation of using the leap-frog Yee scheme [5] on the equations of elastodynamics in the time domain, we let $\mathbf{v} = \partial \mathbf{u}/\partial t$ or $\mathbf{v} = -i\omega\mathbf{u}$. Then, (4) and (5) become

$$-i\omega\rho\mathbf{v} = \nabla_e \cdot \overline{\boldsymbol{\tau}}, \tag{45}$$

$$-i\omega\overline{\boldsymbol{\tau}} = \lambda\overline{\mathbf{I}}(\nabla_e \cdot \mathbf{v}) + \mu(\nabla_e\mathbf{v} + \mathbf{v}\nabla_e). \tag{46}$$

To be of use, the coordinate stretching variables e_x, e_y, and e_z have to be complex. We will let

$$e_x = a_x + \frac{i\Omega_x}{\omega}, \tag{47a}$$

$$e_y = a_y + \frac{i\Omega_y}{\omega}, \tag{47b}$$

$$e_z = a_z + \frac{i\Omega_z}{\omega}. \tag{47c}$$

We have chosen the variables to be frequency dependent for the reason that the Fourier transform of a real-valued function will always have $i\omega$ appearing together.

Consequently, we have

$$-i\omega\rho\mathbf{v}_{sx} = \underline{\partial}_x\hat{x}\cdot\overline{\boldsymbol{\tau}}, \tag{48a}$$

$$-i\omega\rho\mathbf{v}_{sy} = \underline{\partial}_y\hat{y}\cdot\overline{\boldsymbol{\tau}}, \tag{48b}$$

$$-i\omega\rho\mathbf{v}_{sz} = \underline{\partial}_z\hat{z}\cdot\overline{\boldsymbol{\tau}}. \tag{48c}$$

Similarly, we can rewrite (46) as

$$\begin{aligned}-i\omega\overline{\boldsymbol{\tau}} =& [\lambda\overline{\mathbf{I}}\underline{\partial}_x v_x + \mu\underline{\partial}_x(\hat{x}\mathbf{v} + \mathbf{v}\hat{x})] + [\lambda\overline{\mathbf{I}}\underline{\partial}_y v_y + \mu\underline{\partial}_y(\hat{y}\mathbf{v} + \mathbf{v}\hat{y})] \\ &+ [\lambda\overline{\mathbf{I}}\underline{\partial}_z v_z + \mu\underline{\partial}_z(\hat{z}\mathbf{v} + \mathbf{v}\hat{z})].\end{aligned} \tag{49}$$

The above can be rewritten as

$$-i\omega\overline{\boldsymbol{\tau}}_{sx} = [\lambda\overline{\mathbf{I}}\underline{\partial}_x v_x + \mu\underline{\partial}_x(\hat{x}\mathbf{v} + \mathbf{v}\hat{x})], \tag{50a}$$

$$-i\omega\overline{\boldsymbol{\tau}}_{sy} = [\lambda\overline{\mathbf{I}}\underline{\partial}_y v_y + \mu\underline{\partial}_y(\hat{y}\mathbf{v} + \mathbf{v}\hat{y})], \tag{50b}$$

$$-i\omega\overline{\boldsymbol{\tau}}_{sz} = [\lambda\overline{\mathbf{I}}\underline{\partial}_z v_z + \mu\underline{\partial}_z(\hat{z}\mathbf{v} + \mathbf{v}\hat{z})]. \tag{50c}$$

Since $\underline{\partial}_i = \frac{1}{e_1}\partial_i$, we can multiply the (48) and (50) with the corresponding stretching variable from (47) to remove them from the right-hand side of the equations.

Consequently, transforming the resultant equation to the time domain, we have

$$\rho a_x\partial_t\mathbf{v}_{sx} + \rho\Omega_x\mathbf{v}_{sx} = \partial_x\hat{x}\cdot\overline{\boldsymbol{\tau}}, \tag{51a}$$

$$\rho a_y\partial_t\mathbf{v}_{sy} + \rho\Omega_y\mathbf{v}_{sy} = \partial_y\hat{y}\cdot\overline{\boldsymbol{\tau}}, \tag{51b}$$

$$\rho a_z\partial_t\mathbf{v}_{sz} + \rho\Omega_z\mathbf{v}_{sz} = \partial_z\hat{z}\cdot\overline{\boldsymbol{\tau}}, \tag{51c}$$

$$a_x\partial_t\overline{\boldsymbol{\tau}}_{sx} + \Omega_x\overline{\boldsymbol{\tau}}_{sx} = \lambda\overline{\mathbf{I}}\partial_x v_x + \mu\partial_x(\hat{x}\mathbf{v} + \mathbf{v}\hat{x}), \tag{52a}$$

$$a_y\partial_t\overline{\boldsymbol{\tau}}_{sy} + \Omega_y\overline{\boldsymbol{\tau}}_{sy} = \lambda\overline{\mathbf{I}}\partial_y v_y + \mu\partial_y(\hat{y}\mathbf{v} + \mathbf{v}\hat{y}), \tag{52b}$$

$$a_z\partial_t\overline{\boldsymbol{\tau}}_{sz} + \Omega_z\overline{\boldsymbol{\tau}}_{sz} = \lambda\overline{\mathbf{I}}\partial_z v_z + \mu\partial_z(\hat{z}\mathbf{v} + \mathbf{v}\hat{z}). \tag{52c}$$

By the above manipulation, we have avoided convolutions in the above equations as convolutions are expensive to compute. Moreover, the simple finite difference time domain (FDTD) scheme can be used to solve the above equation by time stepping.

5. Numerical Results

To solve the partial differential equations (PDE's) numerically, we need to discretize them accordingly. Even though a perfectly matched interface exists in the continuum space, it does not exist in the discretized space. The discretization error is proportional to the product of the space discretization size and the contrast [23]. Therefore, to minimize the reflection from the grid, we have chosen a parabolic or linear profile for the loss.

We have implemented the codes for both two dimensions as well as three dimensions. We have found the codes to be stable for a homogeneous as well as inhomogeneous medium, as long as the Courant condition is satisfied [22], and the PML ABC works as well if not better than the Liao's ABC.

In the following 2D simulations, the solid has density $\rho = 2200$ kg/m^3, the compressional and shear velocities are: $v_p = 3000$ m/s and $v_s = 1100$ m/s. The fluid properties are: $\rho = 2200$ kg/m^3, $v_p = 1500$ and $v_s = 0$ m/s.

In Figure 1, we show the magnitude field plot of v_x due to a 2D monopole line source radiating at a fluid-solid interface at 100, 150, 300 and 500 time steps. We can see that the field is well absorbed by the material absorbing boundary condition. The simulation region is 60×60 ($\Delta x = \Delta y = 0.008$ m), and the time step is $\Delta t = 1.5 \times 10^{-6}$ s. The source is located at $(0, 0)$, and the interface is located at five grid points above the source. The lower half space is fluid while the upper half space is solid. In this simulation, we have used a 10 grid point PML with parabolic profile and $\Omega_{max}\Delta t = 0.2$. The pulse is a first-derivative Blackman-Harris window pulse with a center frequency of 10 KHz.

Figure 2 shows the plots of the slice of the field through the point (0,0) 100, 150, 300, and 500 time steps. The solid lines are vertical slices while the dotted lines are horizontal slices. We see that the residual field at the late time steps is much smaller than the field at earlier time steps, testing to the stability and quality of the material absorbing boundary condition.

Figure 3 shows the field v_x at $(15, 0)$ up to 500 time steps for the same simulation. No reflection or instability has been observed. We have run the code for as many as 5,000 time steps and have not observed instability for this fluid-solid interface problem.

In Figure 4, we show a 3D FDTD simulation for a homogeneous medium. It shows the comparison of τ_{xx} component obtained by FDTD method with a PML and that with a Liao's boundary condition. For this and next examples, the source function is a second derivative of the Blackman-Harris window function with a center frequency of 5 KHz. Excellent agreement is observed. The computational domain is divided by $N_x \times N_y \times N_z = 50 \times 50 \times 50$ ($\Delta x = \Delta y = \Delta z = 0.0048$ m), and the time step is $\Delta t = 8 \times 10^{-7}$ s. Ten grid points are used for the PML with a linearly increasing attenuation profile. The maximum attenuation at the boundary is $\Omega_{max}\Delta t = 0.2$. The source and receiver are located at grids $(0, 0, 0)$ and $(4, 9, 12)$ respectively.

The next case is a simulation for a 3D inhomogeneous medium with interfaces intersecting computational boundaries. It models a rectangular column of fluid in a solid host, as shown in Figure 5. The fluid has a density of 1000 kg/m^3. The computation domain is gridded by $N_x \times N_y \times N_z = 64 \times 64 \times 64$ ($\Delta x = \Delta y = \Delta z = 0.008$ m), and the time step is $\Delta t = 1.5 \times 10^{-6}$ s. The PML used is the same as the previous case. The source and receiver are located at grids $(0, 0, 0)$ and $(0, 0, 30)$ respectively. Figure 6 shows the comparison of the received pressure waveforms obtained by PML and Liao's ABC. Again, excellent agreement is observed between the two results.

In the last example, we show a simulation for a large problem with three layers of solid penetrated vertically by a fluid column, as shown in Figure 7 which simulates a geophysical well-logging environment. The first and third layers have the same properties as in Figure 5, and the center layer has a density of 2200 kg/m^3, compressional speed of 4000 m/s, and shear speed of 2000 m/s. The layers interfaces are at $z = -0.8$ and $z = 0.8$ m, and a monopole source is located at $(x, y, z) = (0, 0, 0)$. The source function is the first derivative of the Blackman-Harris window function with a center frequency of 5 KHz. The parameters for the fluid column are the same as in Figure 5. An array of receivers are located at grid $(0, 0, 5k)$ with $k = 1, 2, \cdots, 50$. The grid size remains the same as in Figure 5, while the time step has to be reduced to 1.0×10^{-6} s to satisfy the Courant condition. The problem is discretized into $84 \times 84 \times 532$ cells. The received pressure waveforms for 5000 time steps are shown in Figures 8a and 8b. The near field contains large components of direct fluid arrival and higher order waveguide modes, which attenuate rapidly as they propagate. Away from the near field zone and before the layer interfaces, the wavefield is dominated by the Stoneley wave. The compressional head wave is very weak in the center layer. In the upper slower layer, however, one sees a much larger compressional head wave. Two other more dominating wave components, compressional and shear waves, in the upper layer are converted from the Stoneley wave from the center layer at the layer interface. This wave conversion at the layer interfaces is clearly seen in the waveforms. Even with single precision, the solution for this large problem remains stable.

It is noted that the Liao's ABC requires double precision while the PML gives accurate results even with single precision. Taking this factor into account, the PML requires about the same memory as the Liao's ABC. However, the FDTD code with the PML is fully parallelizable.

6. Conclusions

We have proved that a perfectly matched interface exists for linearized elastodynamics. This is easily done from the viewpoint of a stretched coordinate system. We also show how the equations of motion could be split in the time domain in order to incorporate this effect in the time domain. This perfectly matched interface can be used to make perfectly matched layers as absorbers in numerical simulations to emulate an infinite region.

We have demonstrated the feasibility and the stability of such absorbing boundary condition by developing numerical simulation codes in two and three dimensions. The codes are stable and the PML works well even when inhomogeneous medium interfaces intersect with the edge of the simulation region. Such codes are easily developed since only one set of equations needs to be simulated. As such, this method of performing numerical simulation is ideally suited for parallel computation whereby only a single set of codes is required. Also, the code could be run in single precision with no observable instability.

References

1 Alterman, Z., and Kornfeld, P., 1968, Finite difference solution for pulse propagation in a sphere: Israel J. Technology, **6**, 365-371.

2 Ottaviani, M., 1971, Elastic-wave propagation in two evenly welded quarter spaces: Bull. Seism. Soc. Am., **61**, 1119-1152.

3 Boore, D. M., 1972, Finite difference methods for seismic waves: Methods in Computational Physics, 11, Bolt, B. A, Ed., Academic Press Inc., 1–37.

4 Madariaga, R., 1976, Dynamics of an expanding circular fault: Bull. Seism. Soc. Am., **59**, 639–666.

5 Yee, K. S., 1966, Numerical solution of initial boundary value problems involving Maxwell's equation in isotropic media: IEEE Trans. Antennas Propagat., **AP-14**, 302–307.

6 Virieux, J., 1984, SH-wave propagation in heterogeneous media: Velocity-stress finite-difference method: Geophysics, **49**, 1933-1957.

7 Stephen, R. A., Cardo-Casas, F., and Cheng, C. H., 1985, Finite-difference synthetic acoustic logs: Geophysics, **50**, 1588–1609.

8 Randall, C. J., 1989, Absorbing boundary condition for the elastic wave equation: Velocity-stress formulation: Geophysics, **54**, 1141–1152.

9 Randall, C. J., Scheibner, D. J., and Wu, P. T., 1991, Multipole borehole acoustic waveforms: Synthetic logs with beds and borehole washouts: Geophysics, **56**, 1757–1769.

10 Randall, C. J., 1991, Multipole acoustic waveforms in nonaxisymmetric boreholes and formations: J. Acoust. Soc. Am., **90**, 1620–1631.

11 Leslie, H. D., and Randall, C. J., 1992, Multipole sources in boreholes penetrating anisotropic formations: Numerical and experimental results: J. Acoust. Soc. Am., **91**, 12–27.

12 Track, A., Daube, F., and Oristaglio, M., 1992, 3-D cross-well simulation and applications: Proc. 62nd Annual Meeting of Soc. Explor. Geophys., 75–78.

13 Yoon, K. H., and McMechan, G. A., 1992, 3-D finite-difference modelling of elastic waves in borehole environments: Geophysics, **57**, 793–804.

14 Liu, Q.-H., Schoen, E., Daube, F., Randall, C., Liu, H.-L., and Lee, P., 1994, Large-scale 3D finite-difference simulation of elastic wave propagation in borehole environments: 128th Meeting of the Acoustical Society of America, Austin, TX, November.

15 Cheng, N., Cheng, C. H., and Toksöz, M. N., 1995, Borehole wave propagation in three dimensions: J. Acous. Soc. Am., **97**, 3483–3493.

16 Liu, Q.-H., Schoen, E., Daube, F., Randall, C., Liu, H.-L., and Lee, P., A 3D finite difference simulation of sonic logging: submitted for publication.

17 Liao, Z. P., Wong, H. L., Yang, B. P., and Yuan, Y. F., 1984, A transmitting boundary for transient wave analysis: Scientia Sinica A, **27**, 1063–1076.

18 Higdon, R. L., 1987, Numerical absorbing boundary conditions for the wave equation: Math. Comput., **49**, 65–90.

19 Berenger, J.-P., 1994, A perfectly matched layer for the absorption of electromagnetic waves: J. Computational Physics, **114**, 185–200.

20 Chew, W. C. and W. H. Weedon, 1994, A 3D perfectly matched medium from modified Maxwell's equations with stretched coordinates: Micro. Opt. Tech. Lett., **7**, 599–604.

21 Chew, W. C., W. H. Weedon, and A. Sezginer, 1995, A 3-D perfectly matched medium by coordinate stretching and its absorption of static fields: ACES Digest, Monterey, CA, March.

22 Chew, W. C., 1990, Waves and Fields in Inhomogeneous Media, New York: Van Nostrand.

23 Chew, W. C., and J.M. Jin, 1995, "Analysis of perfectly matched layers using lattice EM theory in a discretized world," URSI Digest, p. 338, Newport Beach, June 18-23, 1995.

figure

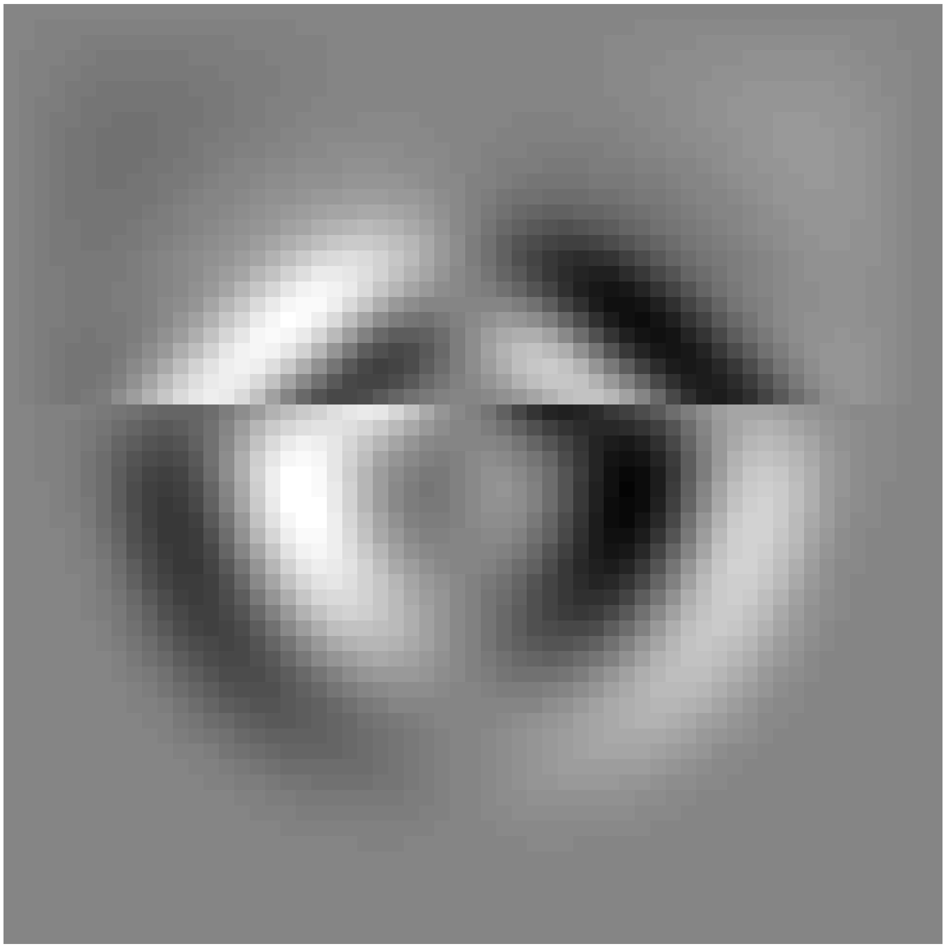

Figure 1a. Magnitude field plot of v_x due to a 2D monopole source radiating at a fluid-solid interface at 100 time steps.

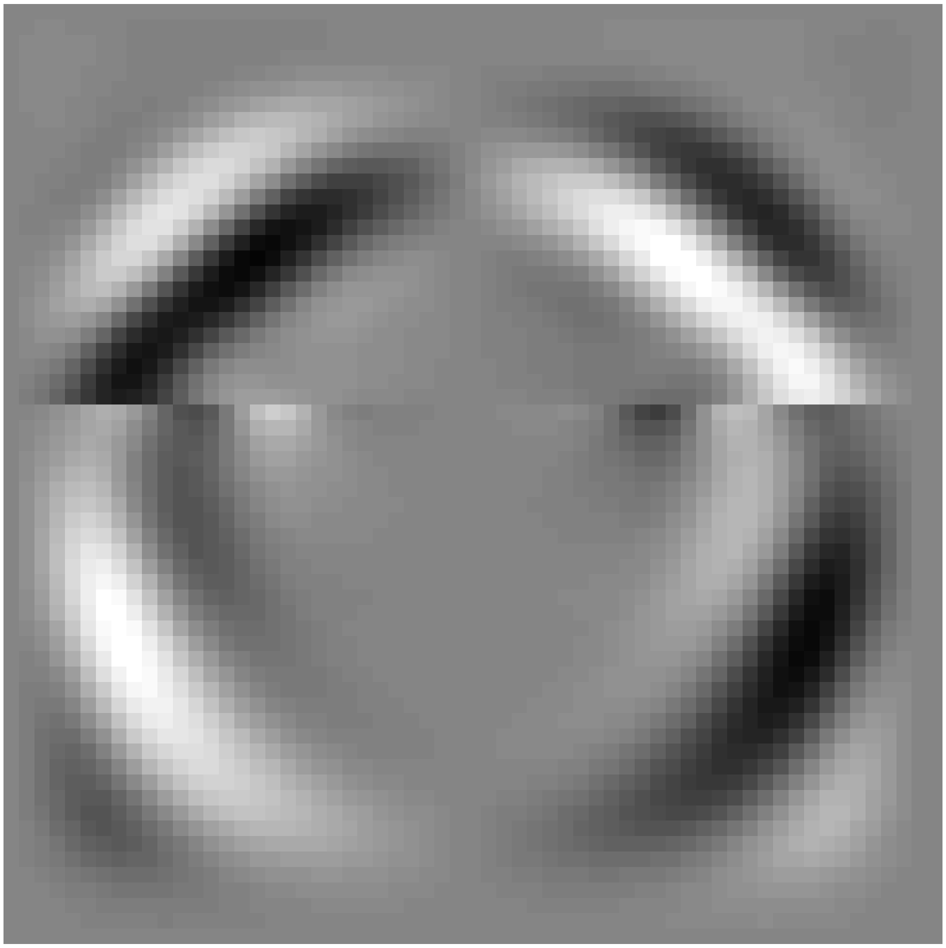

Figure 1b. Magnitude field plot of v_x due to a 2D monopole source radiating at a fluid-solid interface at 150 time steps.

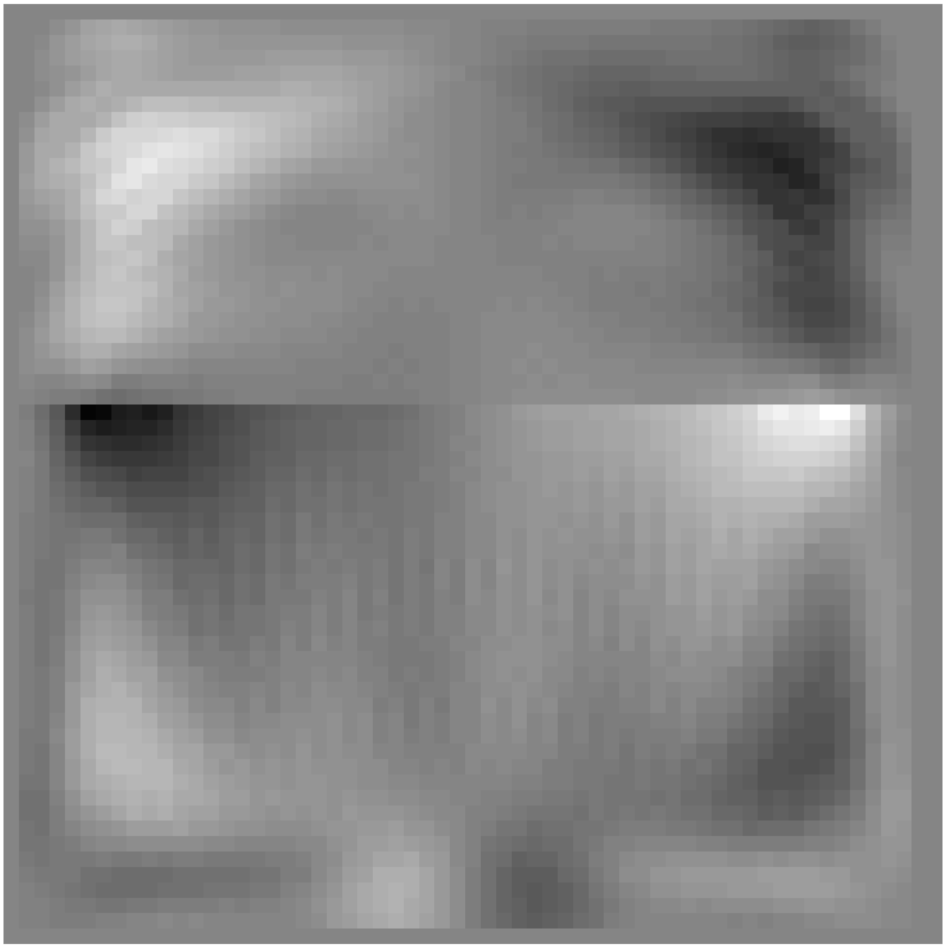

Figure 1c. Magnitude field plot of v_x due to a 2D monopole source radiating at a fluid-solid interface at 300 time steps.

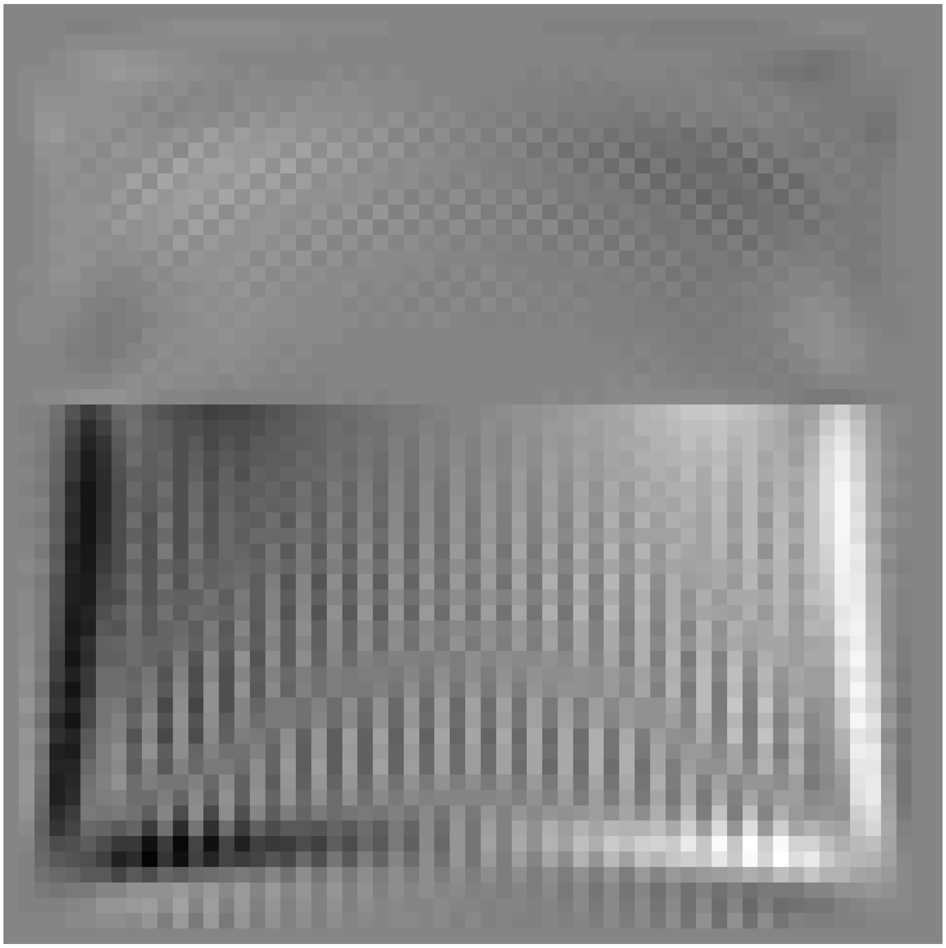

Figure 1d. Magnitude field plot of v_x due to a 2D monopole source radiating at a fluid-solid interface at 500 time steps.

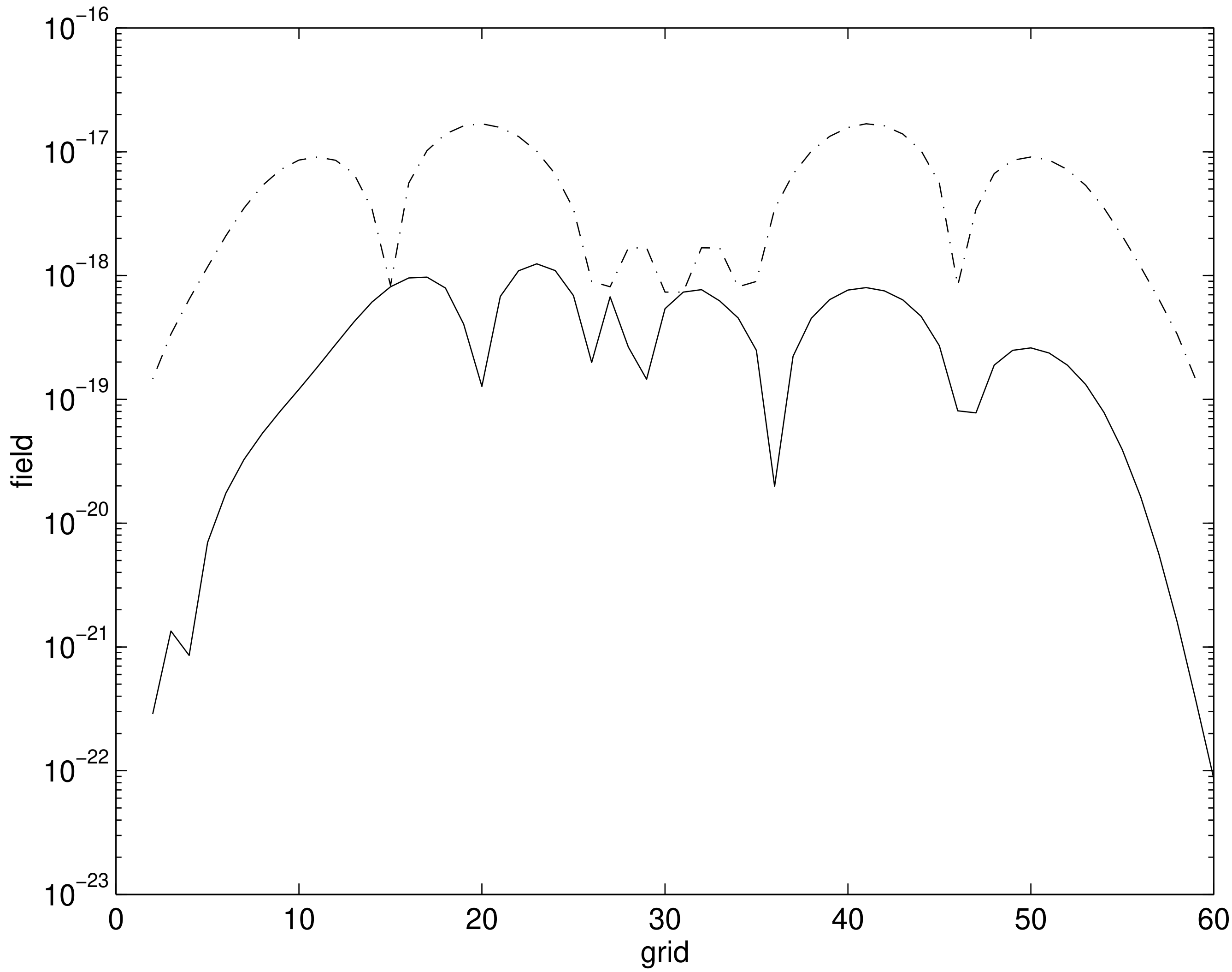

Figure 2a. Plot of the slice of the field through the point (0,0) at 100 time steps. The solid lines are vertical slices while the dotted lines are horizontal slices.

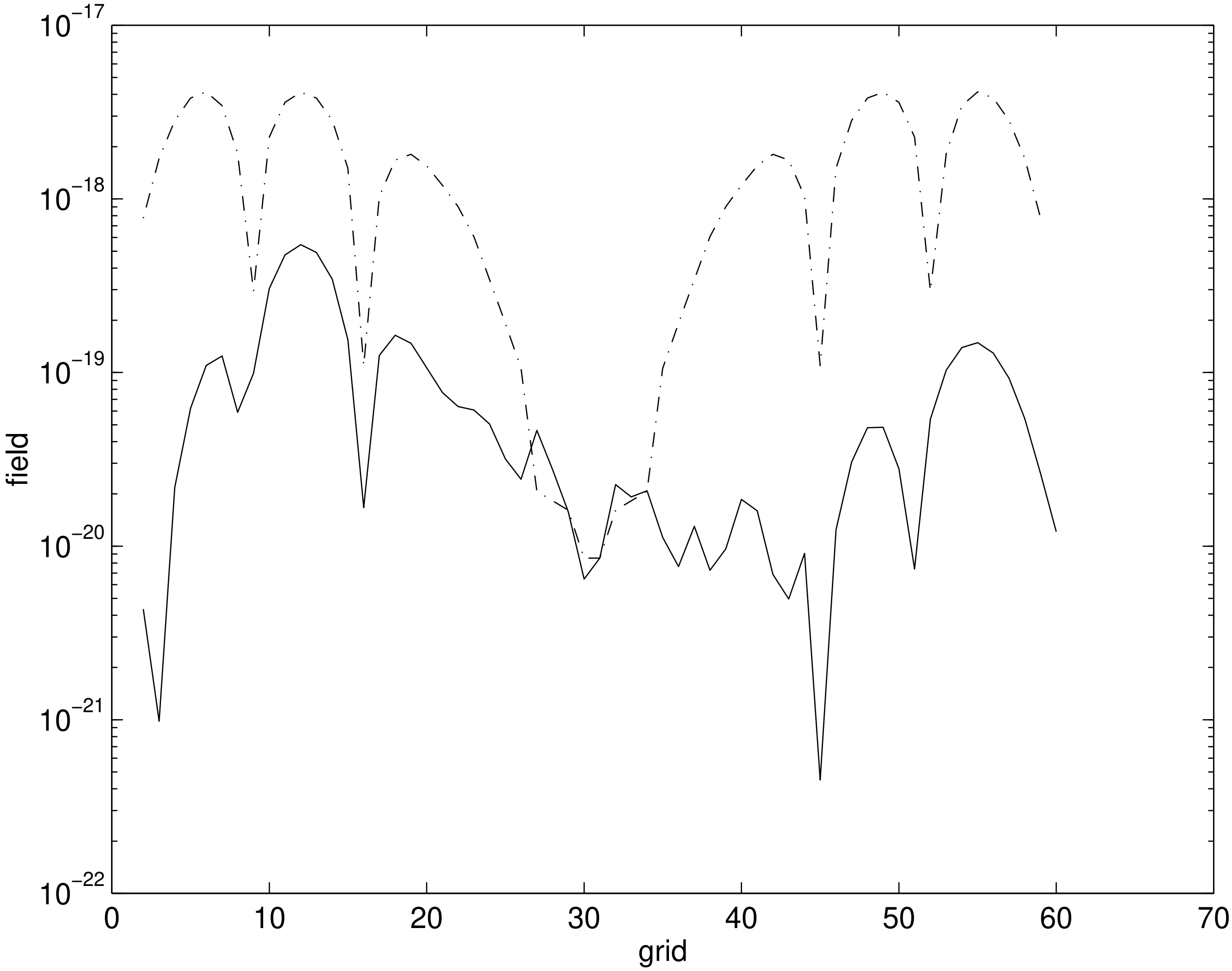

Figure 2b. Plot of the slice of the field through the point (0,0) at 150 time steps. The solid lines are vertical slices while the dotted lines are horizontal slices.

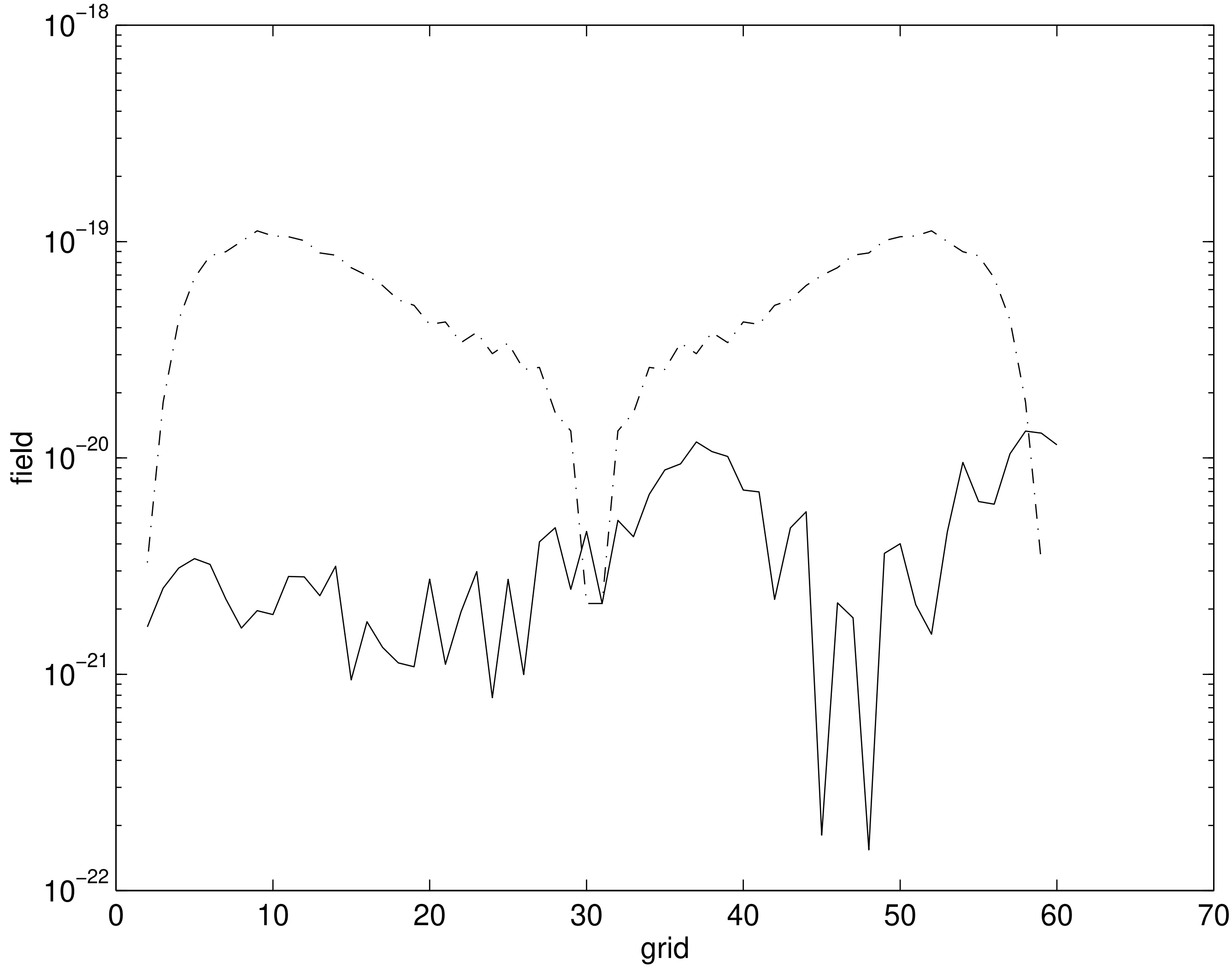

Figure 2c. Plot of the slice of the field through the point (0,0) at 300 time steps. The solid lines are vertical slices while the dotted lines are horizontal slices.

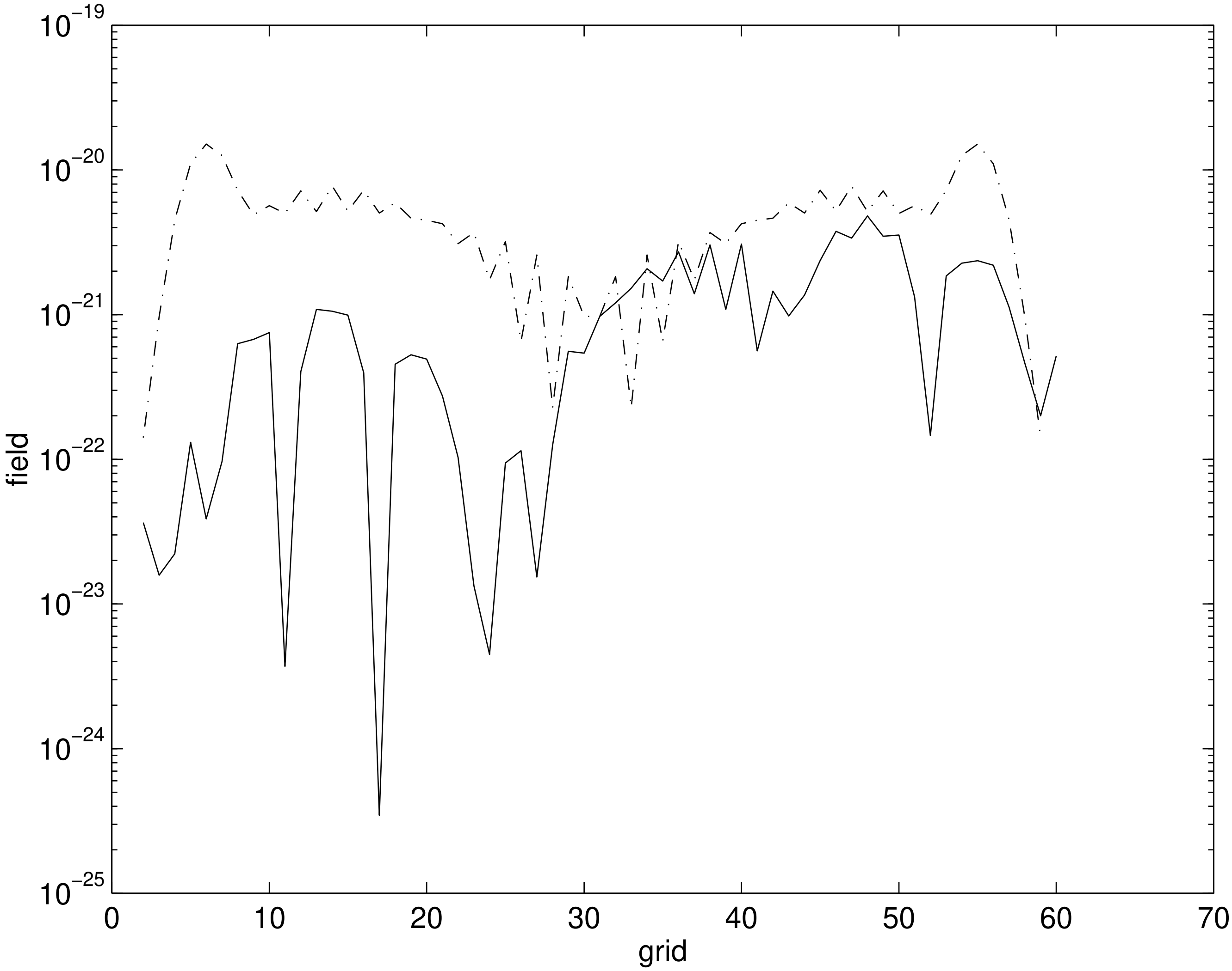

Figure 2d. Plot of the slice of the field through the point (0,0) at 500 time steps. The solid lines are vertical slices while the dotted lines are horizontal slices.

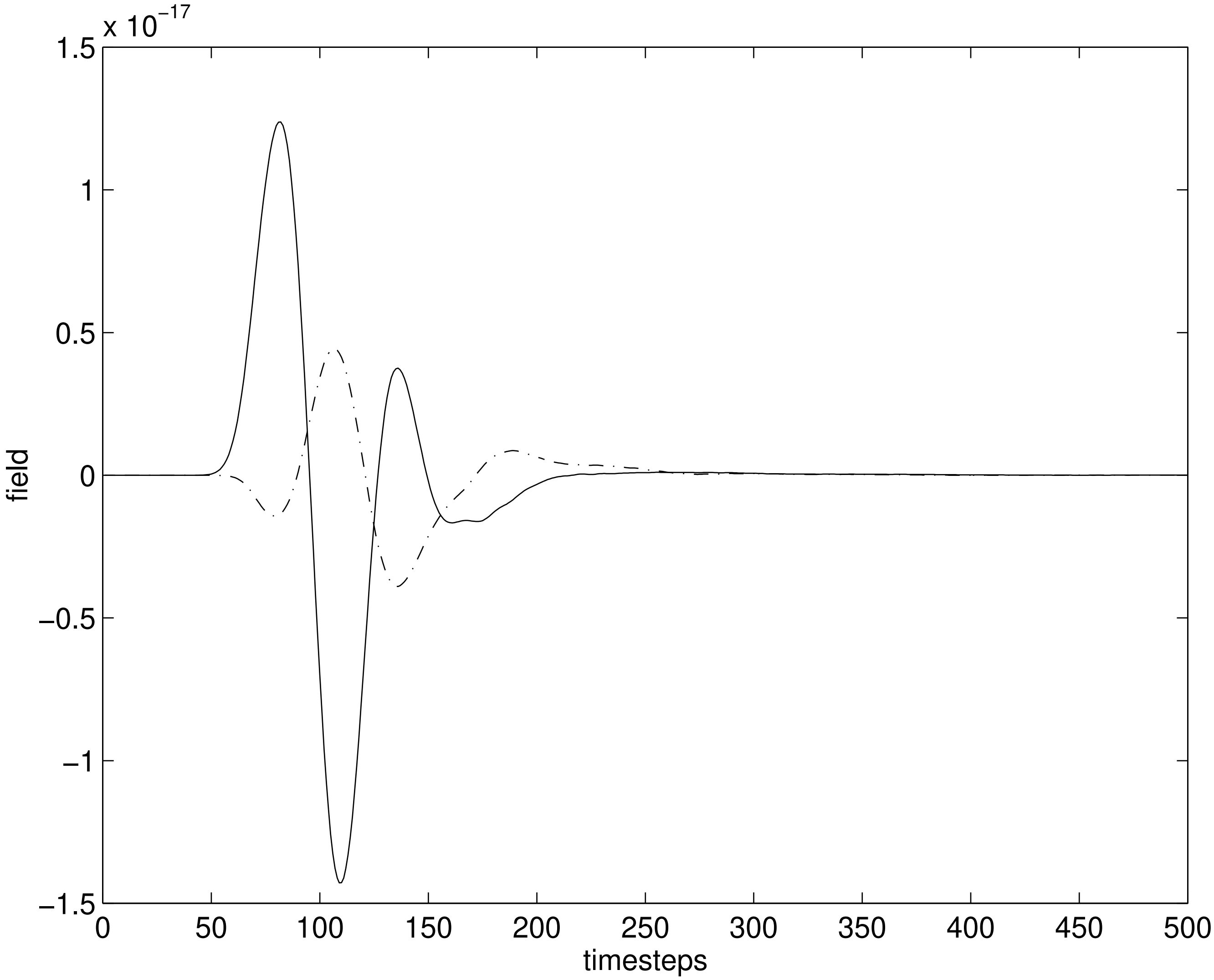

Figure 3. The field v_x at $(15, 0)$ up to 500 time steps for the same simulation as the previous case. No reflection or instability has been observed.

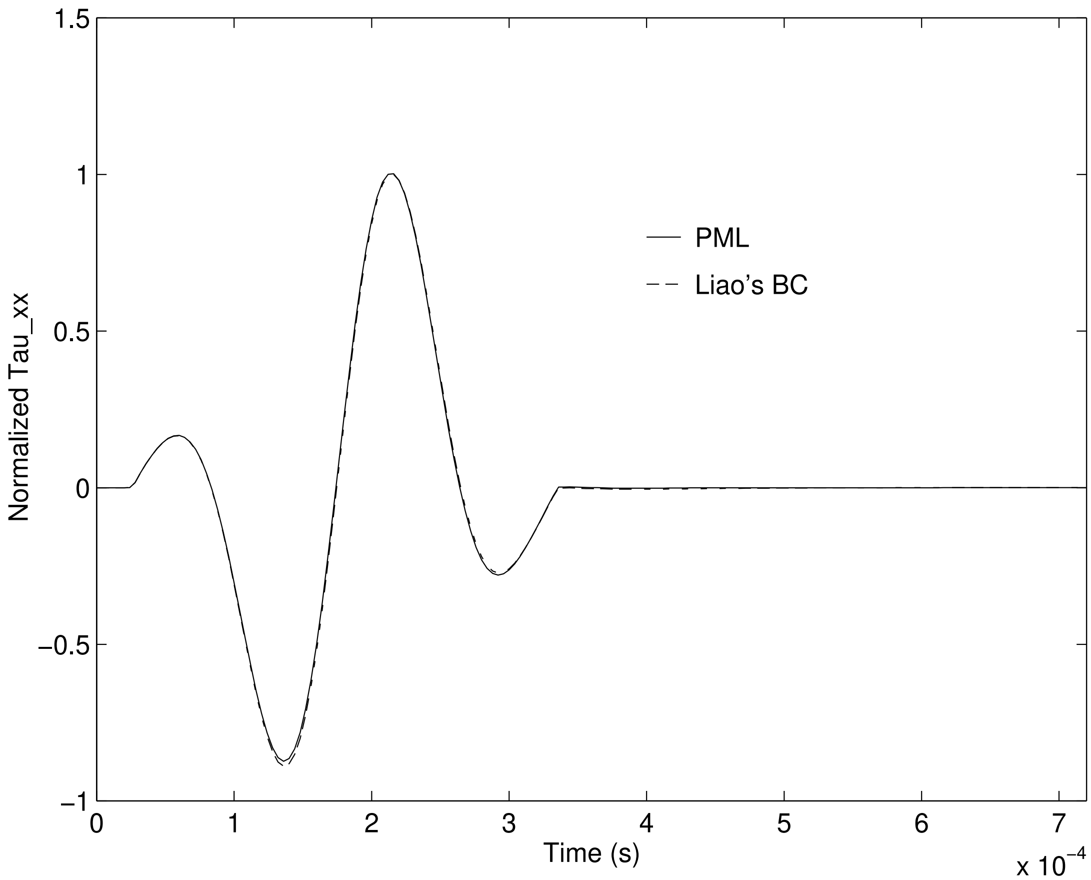

Figure 4. Comparison of PML with Liao's absorbing boundary condition for a homogenesous solid. The source is a monopole, and the receiver is located at grid (4, 9, 12).

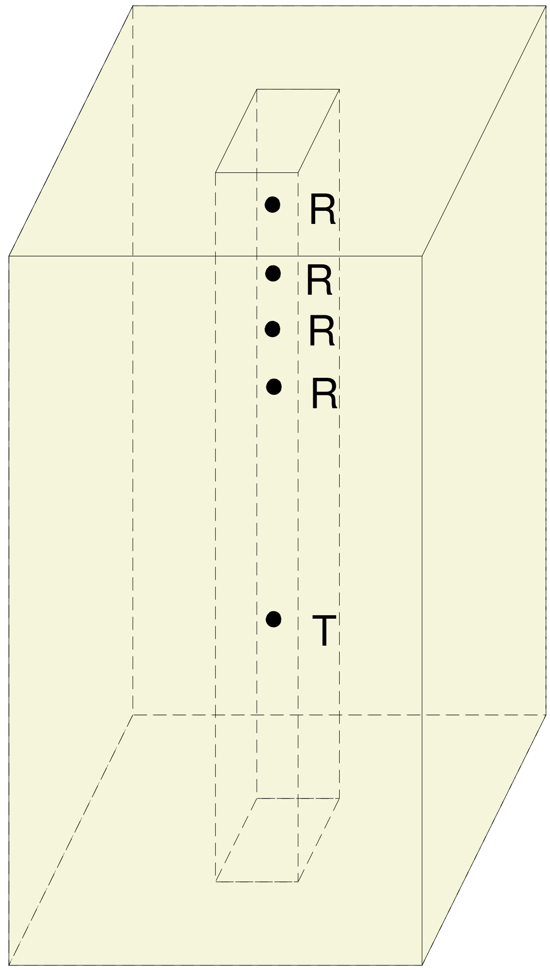

Figure 5. Geometry of a rectangular fluid column in a homogeneous solid host. The cross section of the fluid column is $16 \times 16\ \mathrm{cm}^2$.

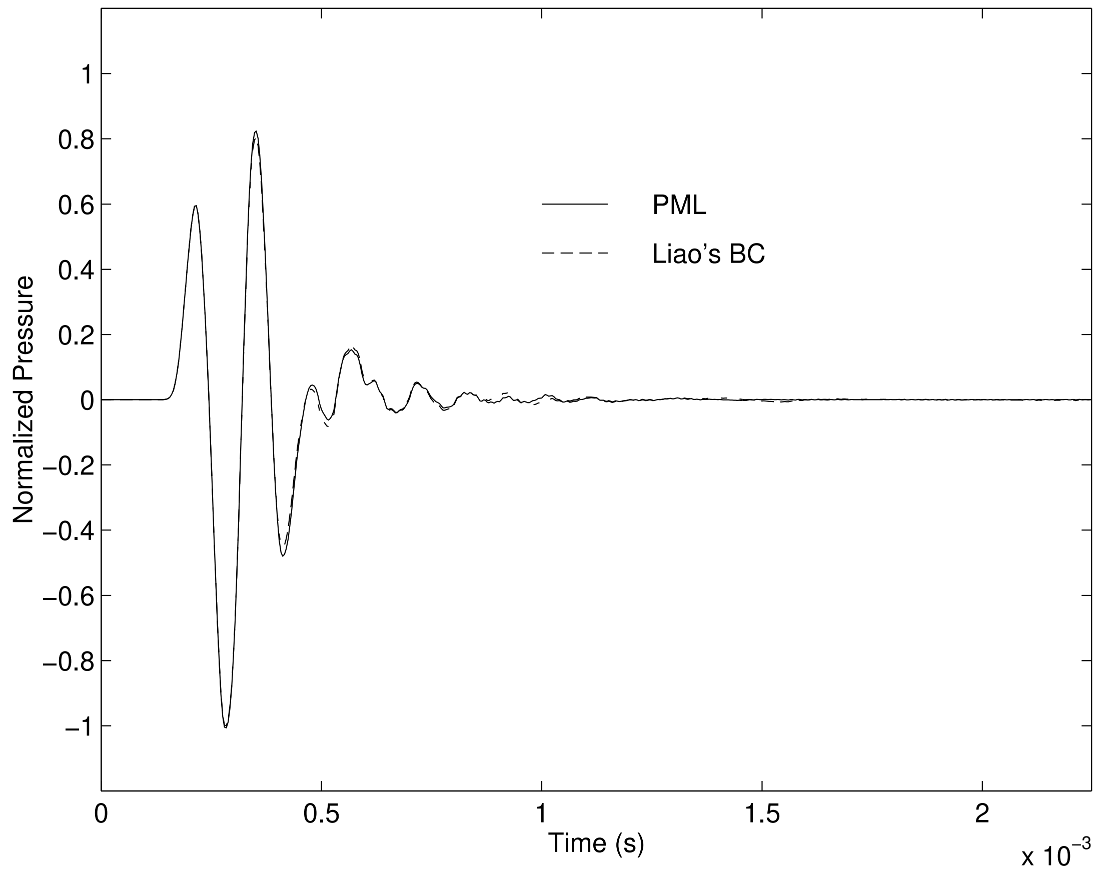

Figure 6. Comparison of PML with Liao's absorbing boundary condition for Figure 5. The source is a monopole, and the receiver is located at grid (0, 0, 30).

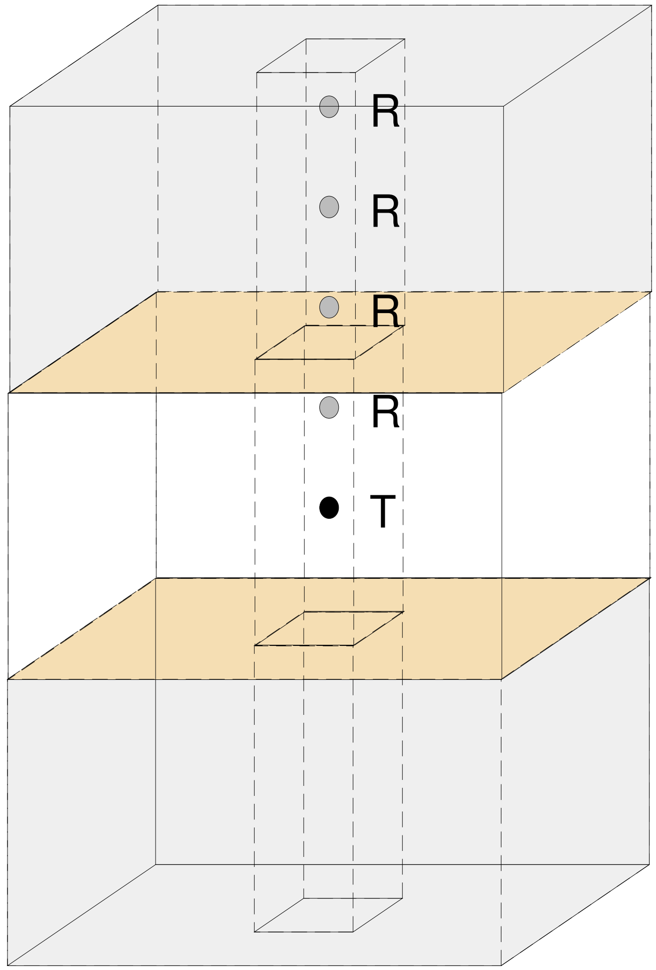

Figure 7. Geometry of a rectangular fluid column in a three-layer solid host for a geophysical well-logging environment. The cross section of the fluid column is 16×16 cm^2, and the thickness of the center layer is 1.6 m. An monopole source is located at the center of the layer.

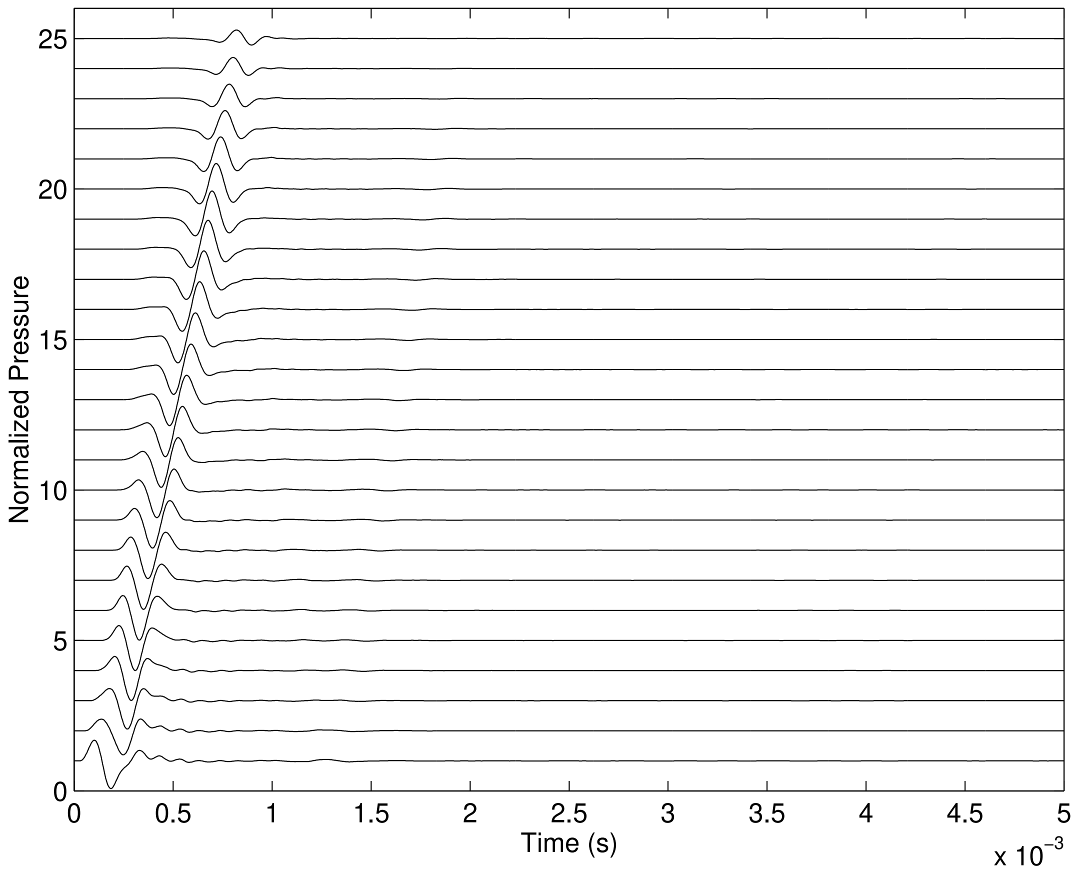

Figure 8a. Pressure waveforms for receivers 1 to 25 for the problem in Figure 7. Waveforms are scaled to the maximum of the first waveform.

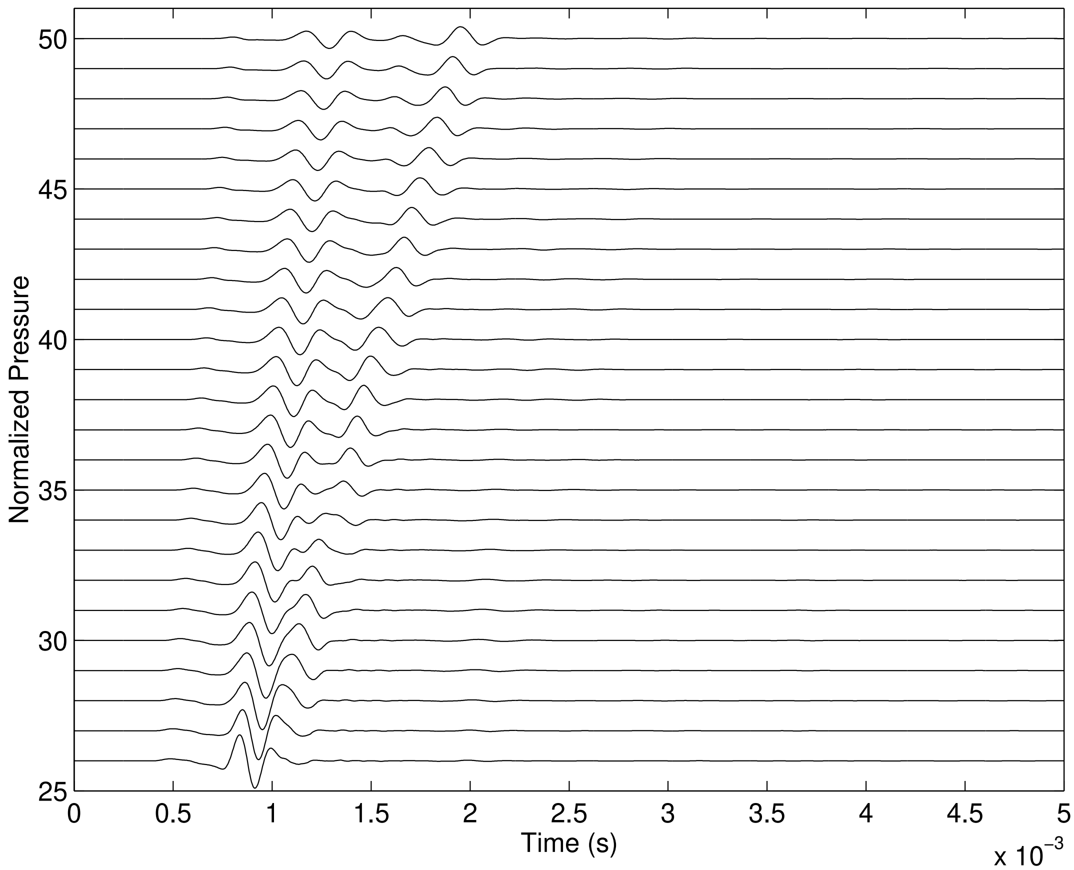

Figure 8b. Pressure waveforms for receivers 26 to 50 for the problem in Figure 7. Waveforms are scaled to 1/4 of the maximum of the first waveform in Figure 8a.